



# Microstructure and Wear Behavior of Cold-Sprayed Cu-BNNSs Composite Coating

Yun Wang<sup>1</sup> · Yiqing Zhu<sup>1</sup> · Ruitao Li<sup>1</sup> · Hongtao Wang<sup>2</sup> · Lihui Tian<sup>3</sup> · Hua Li<sup>4,5</sup>

Submitted: 10 November 2020 / in revised form: 8 May 2021 / Accepted: 29 May 2021  
© ASM International 2021

**Abstract** Cu-boron nitride nanosheets (BNNSs) composite coating was fabricated by mechanical alloying and then cold spray. The microstructure, mechanical properties and tribological performance of the composite coating were investigated. The addition of BNNSs into Cu leads to a decrease in the deposition efficiency and microhardness of the coating. However, the introduction of BNNSs reduces the coefficient of friction evidently and improves the wear resistance significantly (by 34%) due to the sliding and lubricating effects of the BNNSs. Hence, the Cu-BNNSs composite coatings could be excellent candidates for low friction and high wear-resistance applications.

**Keywords** boron nitride nanosheets · Cu-based composite coatings · cold spray · mechanical alloying · wear resistance

## Introduction

Cold spray has broad application prospects in repair, remanufacturing, and 3D additive manufacturing because of its high efficiency and easy scalability (Ref 1-4). During the cold spray process, particles are accelerated to a high velocity and then deposited onto the substrates with strong plastic deformation (Ref 5). Compared with conventional thermal spraying methods, cold spraying has a low processing temperature, which can greatly reduce the deficiencies caused by thermal input such as oxidation, residual tensile stress and chemical reactions (Ref 6-9). Thus, it has become a suitable approach for the deposition of the readily oxidized and heat-sensitive materials (Ref 10-12). In view of these advantages, cold spray is a viable deposition technique for the preparation of ductile metal-based coatings, especially for copper (Ref 9, 13, 14).

Cu-based alloys are widely used as bearing materials, which can reduce friction and wear on the bearing surface (Ref 15-17). However, frequent start and stop will damage the lubricating film and lead to dry friction between the bearing and bushing, which will aggravate the wear of copper-based bushing (Ref 18). Therefore, it is necessary to improve the wear resistance and self-lubricating performance of bearing bush. One solution is to add reinforcements into Cu matrix to form composites or coatings. In recent years, hard ceramic particles were added to cold-sprayed Cu-based coatings to improve the wear resistance. Liuyan et al. Ref 14 studied the tribological behavior of the cold-sprayed method to fabricate Cu-Al<sub>2</sub>O<sub>3</sub> coatings. The results showed that the Cu-Al<sub>2</sub>O<sub>3</sub> coatings exhibited lower wear rate than the Mg alloy substrate. However, the disadvantage of the Cu-based coatings with the addition of hard ceramic reinforcements is the relatively higher friction coefficient than that of the Cu coatings (Ref 10, 19). In

✉ Ruitao Li  
RLI3@e.ntu.edu.sg

<sup>1</sup> School of Mechanical Engineering, Jiangsu University, 301 Xuefu Road, Zhenjiang 212013, Jiangsu Province, China

<sup>2</sup> School of Mechanical and Materials Engineering, Jiujiang University, Jiujiang 332005, China

<sup>3</sup> National Demonstration Center for Experimental Materials Science and Engineering Education, Jiangsu University of Science and Technology, Zhenjiang 212003, China

<sup>4</sup> Key Laboratory of Marine Materials and Related Technologies, Zhejiang Key Laboratory of Marine Materials and Protective Technologies, Ningbo Institute of Materials Technology and Engineering, Chinese Academy of Sciences, Ningbo 315201, China

<sup>5</sup> Cixi Institute of Biomedical Engineering, Ningbo Institute of Materials Technology and Engineering, Chinese Academy of Sciences, Ningbo 315201, China

order to obtain good solid lubricity, some solid lubricants have been added to the coatings. For instance, Chromik et al. Ref 20 deposited a Cu-MoS<sub>2</sub> composite coating by cold spray, and it exhibited a low friction coefficient. Nevertheless, the micron-sized solid lubricant added into Cu matrix might diminish the wear resistance (Ref 21). To solve the incompatibility problem of wear resistance and self-lubricating performance for the cold-sprayed Cu-based coating, it may be a feasible way to add the nanoscale solid lubricant into Cu matrix.

Boron nitride nanosheet is considered as an attractive reinforcement for composites due to its outstanding strength, high thermal conductivity, superb thermal stability and self-lubricating properties (Ref 22-24). Recently, Cu-BNNSs composites have been prepared using spark plasma sintering (Ref 25), which possess improved yield strength, tensile strength and modulus compared with that of the pure Cu. Due to the potential use as bearing materials, their wear resistance properties are also of great interest. BN has been reported to significantly improve the wear resistance of other materials, like Al, Mg and polyether ether ketone (Ref 26-28), because of its superb self-lubricating and wear resistance properties. Thus, it is expected that the addition of BNNSs into Cu can also improve its wear resistance. However, the role of BNNSs in the wear resistance of Cu-based composites has not been verified experimentally.

In this work, BNNSs were added to the Cu matrix to form Cu-BNNSs composite coatings. The effects of BNNSs on the microstructural evolution, microhardness and tribological behaviors of the coating were examined.

## Experimental Procedures

### Preparation of the Feed Powder and Coatings

The procedure of the experiments is schematically shown in Fig. 1. Commercially available hexagonal boron nitride powder (99% purity) with an average particle size of 10 μm and the electrolytic copper powder (99.9% purity) with a size of less than 10 μm were used as starting materials in this study. Both of them were supplied by Beijing Xing Rong Yuan Technology Co. Ltd. BNNSs were obtained through wet milling of h-BN powder in ethanol using stainless steel milling media and with a ball-to-powder weight ratio of 40:1 at 350 rpm for 40 min. In this process, BNNSs were exfoliated from the h-BN powder through the shear and impact forces during ball milling process (Ref 22, 29, 30). The ball milled slurries were sonicated for 2 h and then allowed to stand for 24 h. Finally, the suspension containing BNNSs was taken out and dried in a vacuum dryer. Ball milling method was used

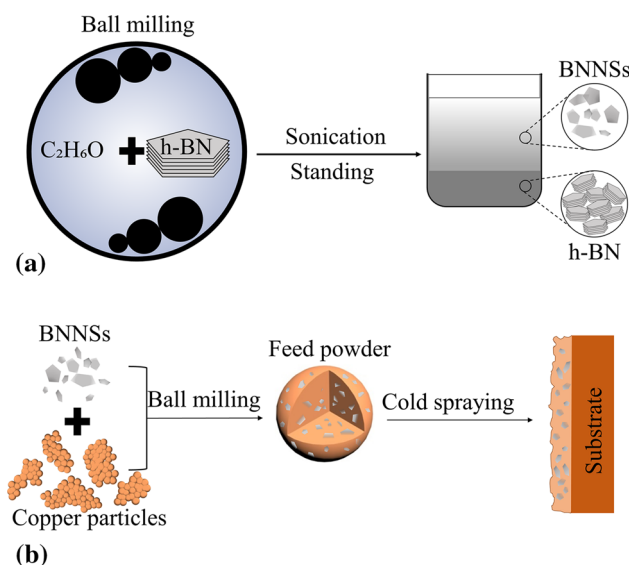


**Fig. 1** Schematic representations of the experimental procedure

**Table 1** Principal parameters used during cold spraying

| Parameters                             | Values |
|--|--------|
| Spraying temperature, °C               | 400±15 |
| Accelerating gas pressure, MPa         | 2.5    |
| Power feed gas pressure, MPa           | 2.8    |
| Spraying gun traversing velocity, mm/s | 50     |
| Standoff distance, mm                  | 20     |
| Number of spraying circles             | 3      |

to disperse 1 wt.% BNNSs in the Cu powder in argon-protected environment for 3 h at 130 rpm with a ball-to-powder weight ratio of 10:1. The ball milled Cu-BNNSs composite powder was then sifted with no.500 and no.1500 wire mesh prior to spraying. For comparison, pure copper was also prepared by the same method.

The cold spray system (CS-2000) was employed to prepare Cu-BNNSs composite coating on the surface of the TU1 copper plate. A spray gun with a converging–diverging de-Laval-type nozzle of a throat diameter of 2 mm was adopted. N<sub>2</sub> was used as the accelerating gas and powder feed gas. The spraying parameters used to deposit the coatings are shown in Table 1. In order to assure a strong bonding between the coating and the substrate, the substrates were blasted with 20 mesh alumina for 30s prior to the cold spray deposition.

### Characterization

The microstructure of the feedstock powder and coating was characterized by Hitachi S-3400 N scanning electron

microscope (SEM), and field emission scanning electron microscopy (JSM-7001F, JEOL, Japan) equipped with an energy dispersive x-ray spectrometer (EDS). High-resolution transmission electron microscope (HRTEM, FEI Tecnai G2 F20) was employed to characterize the BNNSs in detail. Cross-section of the powder particles was prepared according to the standard metallographic method (ASTM E3–11) (Ref 31). The Cu-BNNSs composite powders were cold mounted in EpoFix resin, and then the specimens were ground and polished. The inlaid samples were finally etched by aqueous ferric chloride-hydrochloric acid solution to observe the microstructure. The porosity of the coatings was measured by ImageJ software with 10 scanning electron microscope (SEM) images of 1000× magnification. The phase of the milled powder and coatings was identified by an x-ray diffraction (D8 ADVANCE, BRUKER, Germany) with Cu K $\alpha$  radiation at a step of 1°. The microhardness was measured with Vickers hardness testing machine (HXS-1000TAC, Shoufeng, Shanghai, China) with the load of 100 g for 15 s. Forty measurements were taken from each sample for statistical analysis. In order to reduce the influence of surface roughness on microhardness, all the tested samples were polished carefully before the microhardness test.

A rotating ball-on-disk tribometer (HT-1000, China) was used for the wear test. Before this test, each specimen was ground using #5000 abrasive paper and then polished using diamond slurries down to an average surface roughness (Ra) of 0.3  $\mu\text{m}$ . GCr15 ball with a diameter of 6 mm was used as the counterparts, which was sonicated in ethanol to remove any contaminants. The applied load is 4 N under the frequency of 560 rpm with a rotating radius of 3 mm for 15 min. All the tribological tests were performed in the air environment at room temperature. For each sample, the wear tests were repeated three times to get an average wear rate. The wear rate was calculated by the wear equation of  $W=V/(S\cdot L)$ , where W, V, S and L are wear rate ( $\text{mm}^3\cdot\text{N}^{-1}\cdot\text{m}^{-1}$ ), wear volume ( $\text{mm}^3$ ), load (N) and sliding distance (m), respectively. The wear volume of tested coatings and the surface profiles of the as-sprayed samples was obtained by a confocal laser scanning microscope (VK-X200, Keyence, Japan).

## Results and Discussion

### Microstructure of Feed Powder

Figure 2 shows the morphology of the pristine Cu, BNNSs and Cu-BNNSs composite powder. It can be seen that the pristine Cu powder (Fig. 2a) had a size from 5  $\mu\text{m}$  to 10  $\mu\text{m}$  with globular protrusions on the surfaces. Figure 2(b) shows a typical HRTEM image of the exfoliated

BNNSs by a combination of ball milling and sonication. Due to ultimately thin shapes, the BNNSs were semi-transparent when irradiated by the electron beam. There were scratches and wrinkles on the surface of ultrathin 2D BNNSs. The individual BNNS has an average size of 0.7  $\mu\text{m}$   $\times$  0.7  $\mu\text{m}$  and a thickness of approximately 20 nm. Unlike as-received Cu powder, the Cu-BNNSs composite powder (Fig. 2c) had a flake-like shape with sharp edges and flat surfaces. The inset in Fig. 2(c) shows that BNNSs were well dispersed on the surface of Cu particles. Figure 2(d) is a micrograph of the cross-section of composite powder (Cu-BNNSs). It can be seen that Cu-BNNSs composite powder showed a lamellar microstructure due to intensive collision and cold-welding effect during ball milling process and BNNSs were embedded into Cu matrix. In addition, some discrete BNNSs could be observed between the layers as indicated by the white arrows (Fig. 2d).

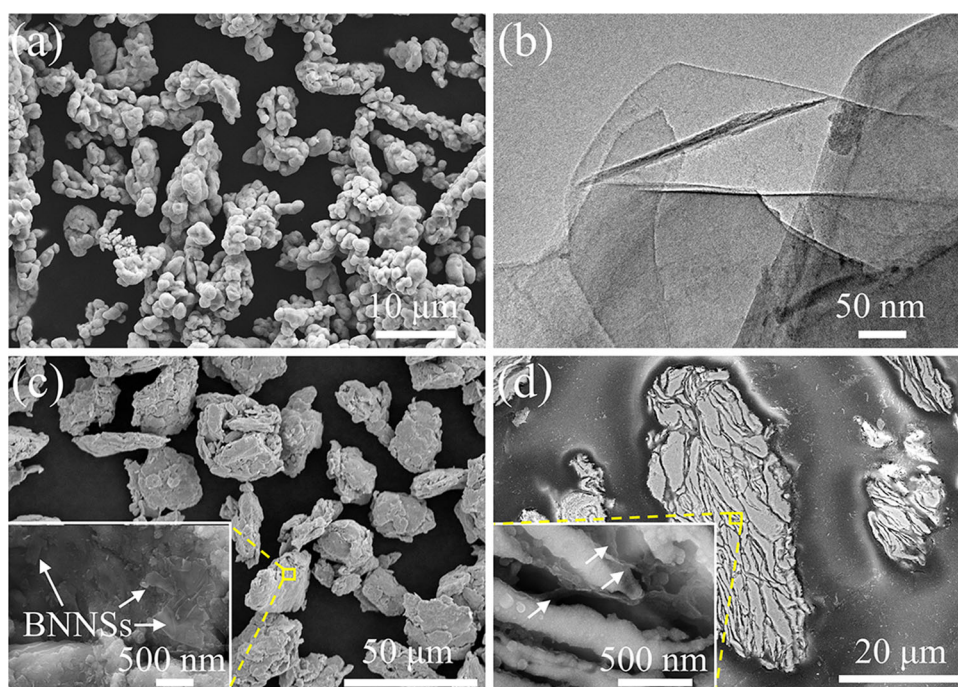
### Coating Morphology and XRD

Figure 3(a) and (b) show the cross-sectional SEM image of pure Cu and Cu-based composite coating on Cu substrate. It is found in Fig. 3(a) that the pure copper coating has a dense microstructure (porosity:  $\sim 0.8\%$ ) and a thickness of  $890 \pm 60 \mu\text{m}$ . Nevertheless, when the BNNSs were added into copper powder, the porosity of cold-sprayed Cu-BNNSs composite coating is as high as  $\sim 2.6\%$ . Additionally, the thickness decreased to  $620 \pm 34 \mu\text{m}$ . This agrees well with Edward's and Wenyuan's findings (Ref 9, 10) that nanosheets can reduce the deposition efficiency. Pores were distributed between deformed particles, which was caused by the poor deformation between the deposited particles.

Due to their brittle nature, Cu-BNNSs composite coatings were bent 60 degrees using a thimble moving at a speed of 0.1 mm/s to create fracture surfaces, which were used to evaluate the distribution and state of BNNSs in the coatings. Figure 3(c) presents the schematic diagrams of bending the samples and the fractured sample. Figure 3(d) shows the fracture surface of Cu-BNNSs coating. It seems that de-cohesive rupture occurred in the coating, as no pit was observed. In addition, many BNNSs were seen on the particle boundaries, as marked with white arrows in Fig. 3(e).

The deformation and bonding behavior of two types of particles is schematically shown in Fig. 4. In the deposition process, Cu particles could deform freely with unaffected adiabatic shear (Fig. 4a), while BNNSs may hinder the local adiabatic shear of the composite particles and weaken their bonding, even making some particles rebound (Fig. 4b). This resulted in a higher porosity and lower deposition rate of the composite coating.

**Fig. 2** Morphology of feedstock: (a) Cu; (b) BNNSs; (c) Cu-BNNSs Composite powder; (d) cross-section of composite powder (Cu-BNNSs)



The surface micrography and 3D topographies of the cold spray coatings are shown in Fig. 5. The surfaces of the coatings displayed plateau-like and crater-like features. However, there is a clear difference in the surface roughness between the two coatings. The arithmetical mean height ( $S_a$ ) and average maximum height ( $S_z$ ) of the pure Cu coating were around  $28\ \mu\text{m}$  and  $220\ \mu\text{m}$  (as shown in Fig. 5a and b), while those of the Cu-BNNSs composite coating reduced to  $14\ \mu\text{m}$  and  $125\ \mu\text{m}$  (as shown in Fig. 5c and d). It can be inferred that the existence of BNNSs on the particle surface weakens the deposition ability of particles. Some Cu-BNNSs composite particles played a role of “shot peening”, making the coating surface be tamped.

The XRD spectra of the Cu powder, Cu-BNNSs powder, pure Cu coating and Cu-BNNSs composite coating are exhibited in Fig. 6. The diffraction peaks of the XRD patterns clearly exhibit the cubic structure of Cu. Furthermore, there were no conspicuous variation of XRD patterns of the ball milled powders and coatings. This suggests that the manufacturing process did not result in evident oxidation or phase transformation, thus making cold spray advantageous over other thermal spray technologies like plasma spraying, high velocity oxy-fuel spraying, etc. As reported in previous studies (Ref 24, 32), the XRD patterns of pure BNNSs have peaks at  $26.4^\circ$ ,  $41.5^\circ$ ,  $55.1^\circ$  and  $76.0^\circ$ . However, the peaks of BNNSs became inconspicuous when a low volume fraction of BNNSs and copper was mixed.

### Microhardness

Figure 7(a) shows the microhardness of Cu substrate, Cu coating and the composite coating. The average microhardness value of Cu coating ( $138.9\ \text{HV}_{0.1}$ ) is higher than that of Cu substrate ( $100.8\ \text{HV}_{0.1}$ ), as a result of intense work hardening. However, the hardness of the Cu-BNNSs composite coating ( $119.2\ \text{HV}_{0.1}$ ) was slightly lower than that of the pure Cu coating. This is consistent with Hongyan’s and Wen’s findings (Ref 33, 34) that nanosheets may reduce the microhardness when used as reinforcement of composite materials. Nagabandi et al. Ref 35 fabricated Ag-BNNSs composites via co-electrodeposition/chemisorption and found that the composite hardness tended to decrease due to the BNNSs weakened the contact area between matrix particles. In the present study, the presence of BNNSs disrupted the bonding between Cu particles and increased the porosity of the coating slightly. Indentation stress promoted the detachment between BNNSs and Cu particles. Comparing the indents from the two deposits—with and without BNNSs as revealed in Fig. 7(b) and (c), microcracks were observed around the indentation of Cu-BNNSs composite coating. It could be inferred that a weak binding of BNNSs to the matrix would lead to particle de-bonding (limited interfacial bonding) (Ref 20) and thus reduced the hardness.

**Fig. 3** The cross-sectional micromorphology: (a) Cu coating, (b) Cu-BNNSs composite coating; (c) schematic diagrams of bending the samples and the fractured sample; the fracture surface of the Cu-BNNSs composite coating: (e) low magnification, (f) high magnification

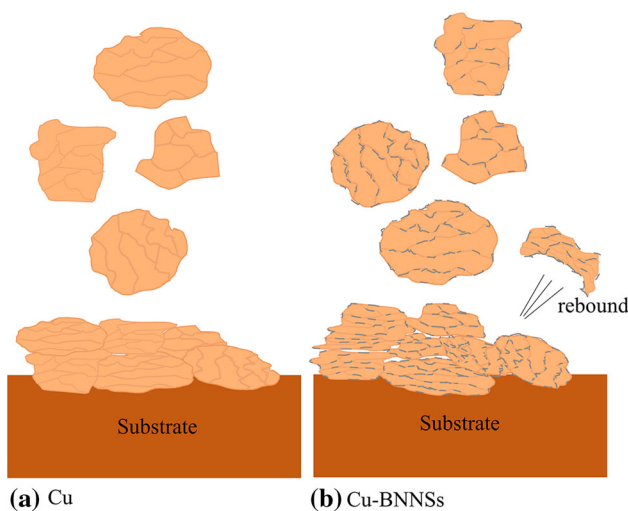
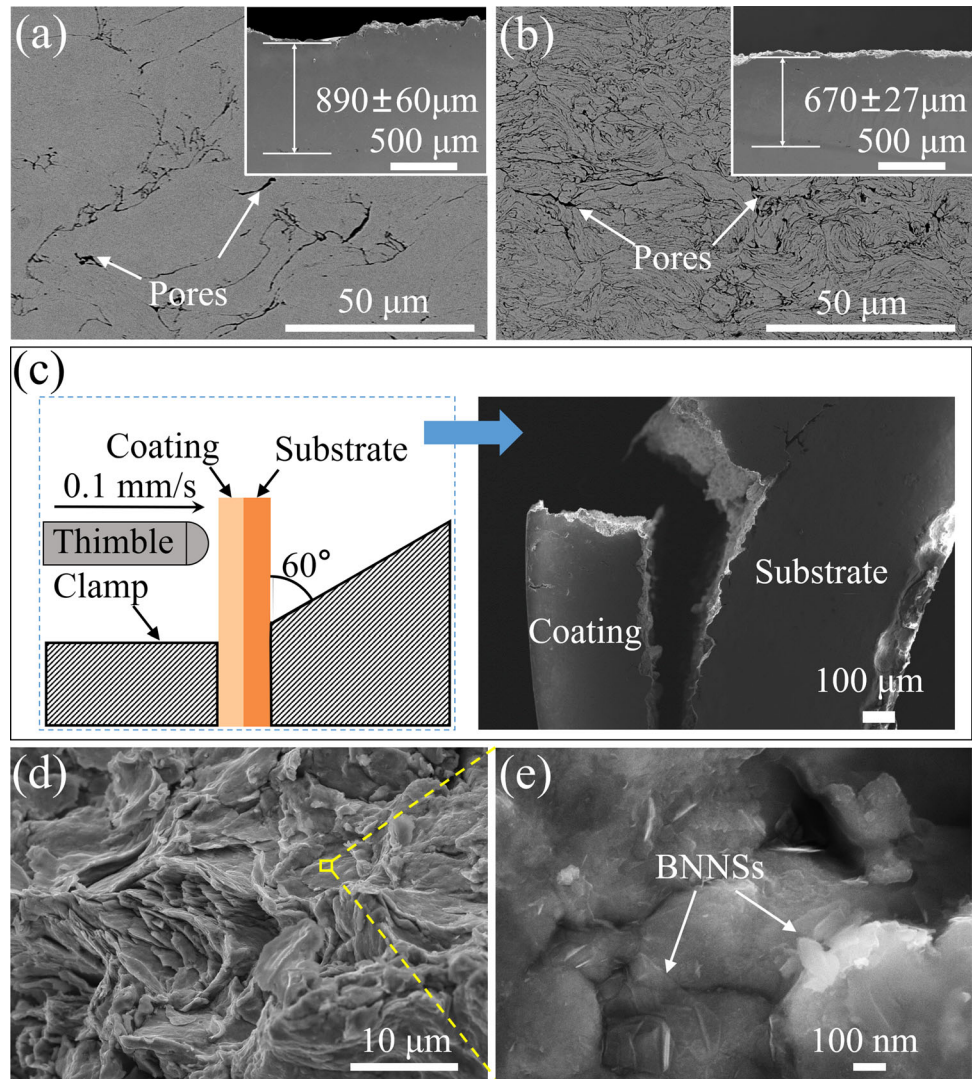


**Fig. 4** Schematic diagram showing the impact behavior of (a) Cu, (b) Cu-BNNSs

### Wear and Tribological Behavior of the Cu-BNNSs Composite Coating

Figure 8(a) shows the coefficients of friction (COFs) of the Cu substrate, Cu coating and Cu-BNNSs composite coating. For the Cu substrate, the COF increased to a high value (about 0.95) in the first 0.5 min and then decreased and finally stabilized. The variation of COF of Cu coating in the testing cycle is very complex. It experienced first a sharp increase and then a moderate decrease followed by a steady rise with large fluctuation and finally stabilization. By contrast, the change of COF of the Cu-BNNSs coating is quite simple. It stabilized immediately after a short rising period. Cu-BNNSs coating had a COF of  $0.51 \pm 0.01$  during stable wear stage, lower than those of the pure copper coating ( $0.76 \pm 0.02$ ) and the Cu substrate ( $0.57 \pm 0.01$ ). In general, the addition of BNNSs resulted in a smaller fluctuation of COF and a lower COF in the steady state friction period of the composite coating. This reflects

**Fig. 5** SEM images and 3D topographies of the surfaces of the coatings

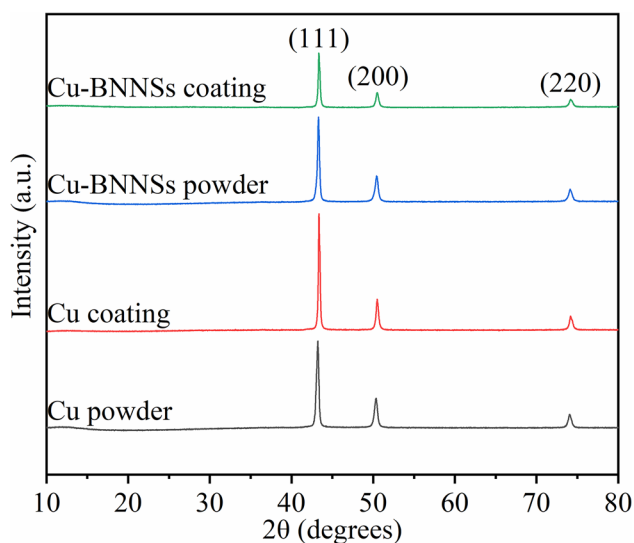
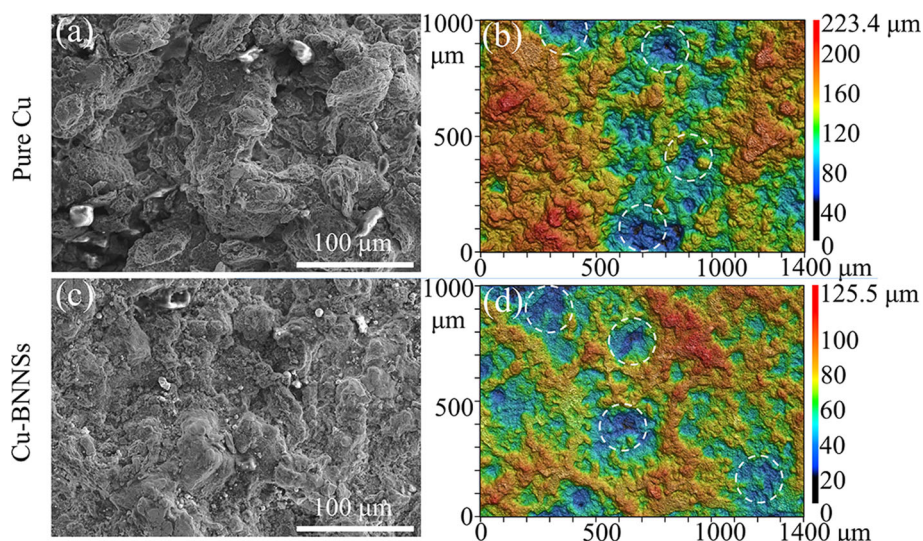


**Fig. 6** XRD spectra of powders and coatings

the improved lubrication of the composite coating and the reduced frictional forces, which was attributed to the presence of the BNNSs.

The comparison of the wear rates of the Cu substrate and coatings is presented in Fig. 8(b). The wear rates of the coatings are lower than that of Cu substrate: the values of Cu coating and Cu-BNNSs coating are around 0.86 and 0.69 of that of Cu substrate, respectively. This indicates that the cold-sprayed coatings can be employed to improve the wear resistance of Cu. It is worth to mention that the wear rate of Cu-BNNSs coating is about 20% lower than that of Cu coating, despite the composite coating yielding lower surface hardness values. Table. 2 compares the wear rate of our coating with those published in recent reports

(Ref 10, 14, 36). It can be seen that the Cu-BNNSs coating exhibited better wear resistance compared with that of the reported Cu-based cold spraying coatings.

To investigate the friction and wear mechanisms of the samples, the SEM images and EDS mapping were employed (Fig. 9). For the Cu substrate, its worn surface is characterized with large wear debris, fracturing, deep grooves and plastic deformation (Fig. 9a1-a3). The accumulation of stress during the friction test led to the propagation of cracks, and the material was finally removed from the contact surface in the form of delamination. Besides, repeated sliding of the delaminated layers results in the formation of deep grooves. This suggests that the Cu substrate suffered adhesive wear and severe abrasion wear (Ref 37, 38), which resulted in high wear rate. The wear characteristics of the Cu coating were presented in Fig. 9(b1-b3). Clearly, the tracks were distinct from those of the substrate. Few debris were present on the track of Cu substrate, while there were many fine debris on the wear track of Cu coating. This can be attributed to the hardness and brittleness of Cu deposit. In addition, features such as debris, abrasive grooves and delaminated scar can also be observed (Fig. 9b3), which indicates micro-abrasion and delamination mechanisms operating simultaneously in Cu coating (Ref 39). The arithmetical mean height ( $S_a$ ) of the wear tracks of the substrate, Cu coating and Cu-BNNSs composite coating was 3.41  $\mu\text{m}$ , 4.19  $\mu\text{m}$  and 2.97  $\mu\text{m}$ , respectively. By contrast, as shown in Fig. 9(c1-c3), the wear track of the Cu-BNNSs coating was smooth with fewer grooves, debris and delamination, indicating the milder wear. Figure 9(a4, b4, c4) shows the EDS mapping of the wear tracks. It reveals that the oxygen content is higher in the worn region of Cu coating than in Cu-BNNSs coating. This suggests that the protective film of BNNSs, which avoids the oxidation of the worn surface.

**Fig. 7** (a) Microhardness of Cu substrate, Cu coating and Cu-BNNSs composite coating, and (b, c) optical micrographs showing Vickers indents on (b) Cu coating and (c) Cu-BNNSs composite coating

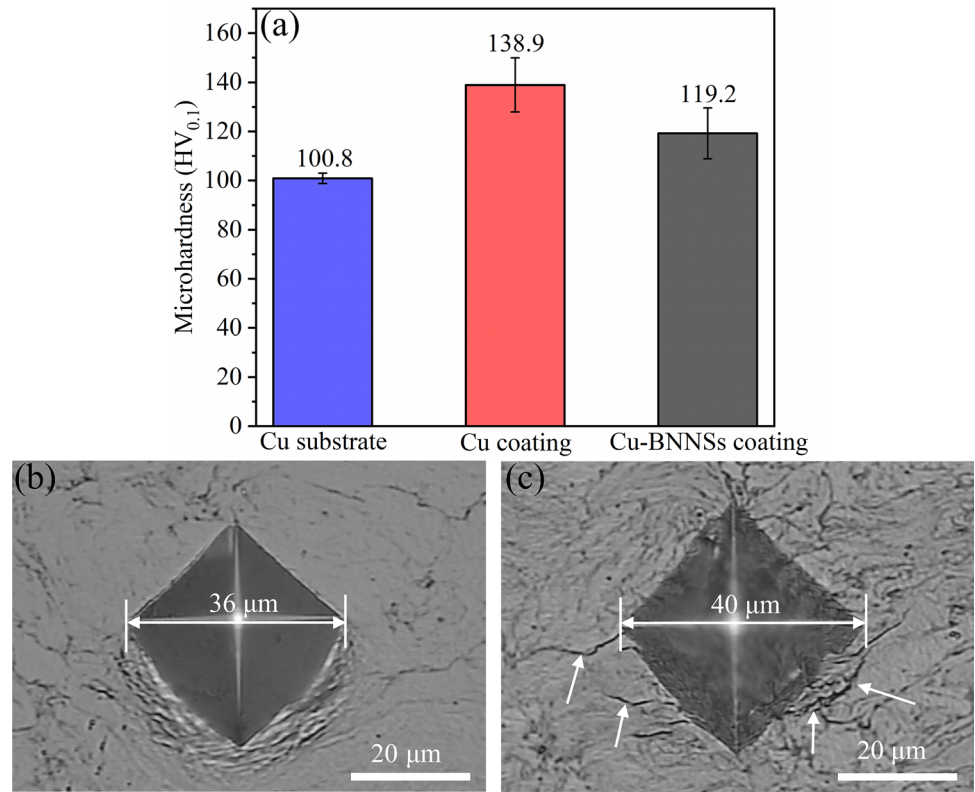


**Fig. 8** (a) Friction coefficients and (b) wear rates of Cu substrate, Cu coating and Cu-BNNSs composite coating

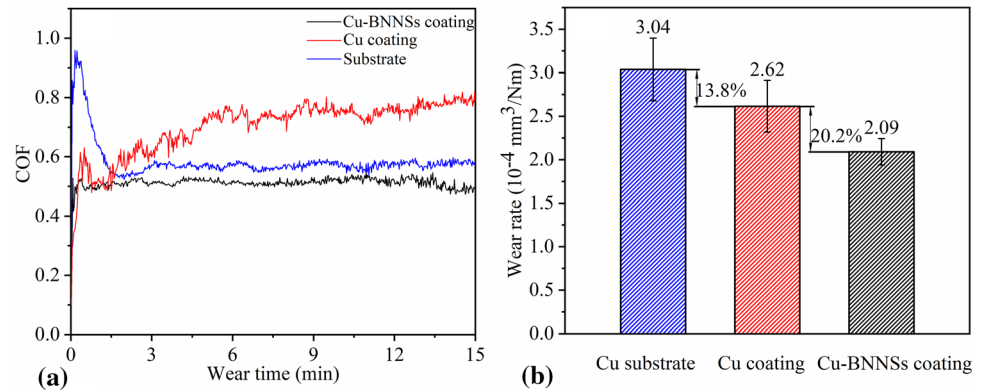
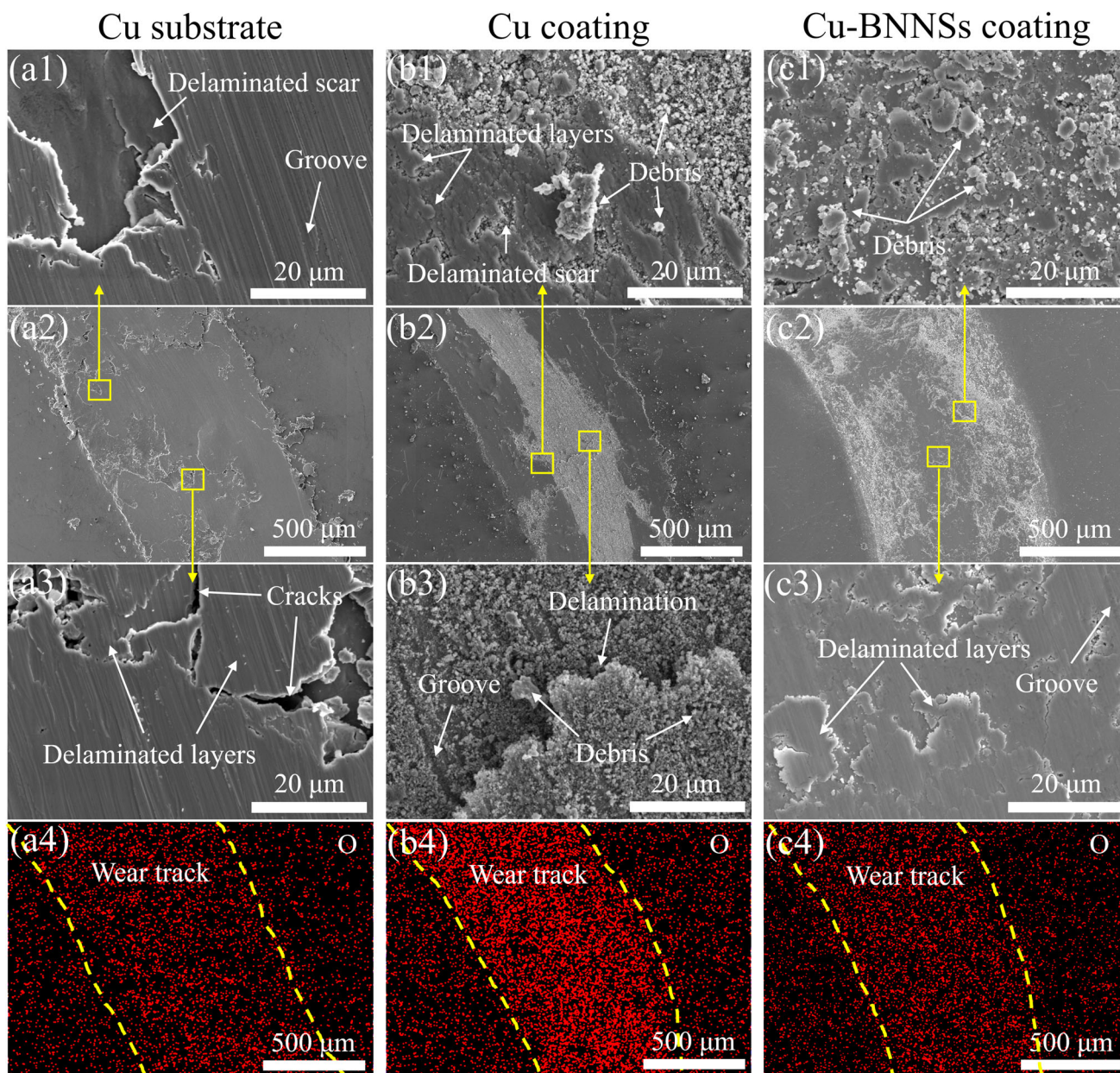


**Table 2** Comparison of wear rate of copper-based cold spraying coatings

| Coatings   | Wear rate, mm <sup>3</sup> /N m | Ref       |
|--|---------------------------------|-----------|
| Cu-45wt.%Al <sub>2</sub> O <sub>3</sub>                          | ~ 8.7 × 10 <sup>-4</sup>        | [14]      |
| Cu-10wt.%Al <sub>2</sub> O <sub>3</sub> -5wt.%Cu-coated graphite | ~ 2.5 × 10 <sup>-4</sup>        | [10]      |
| Cu-5wt.%Cu-coated graphite                                       | ~ 10.2 × 10 <sup>-4</sup>       | [36]      |
| Cu-1wt.%BNNSs  | ~ 2.1 × 10 <sup>-4</sup>        | This work |

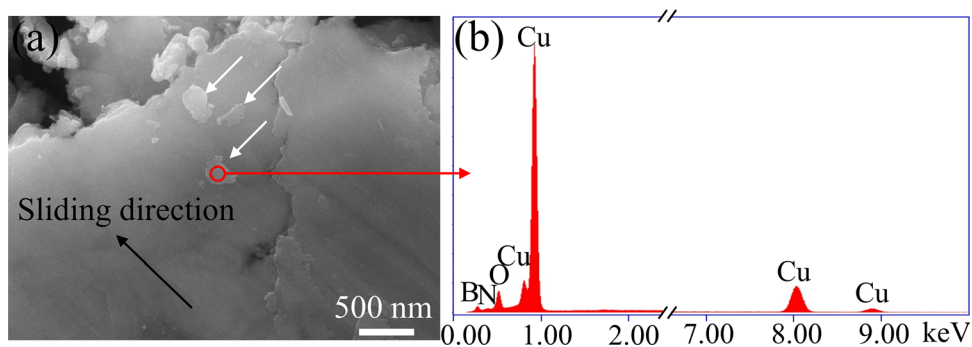
Figure 10 shows the SEM image of BNNSs on the worn surface and the corresponding EDS analysis. Some flat sheets are present on the worn surface, as indicated by the white arrows in Fig. 10(a). The element analysis (Fig. 10b)

of the sheets shows that boron and nitrogen together with Cu exist at the selected zone. Obviously, Cu was due to the signal from Cu matrix, as the area covered in the analysis



**Fig. 9** SEM images and EDS mapping of the wear tracks: (a1, a2, a3, a4) Cu substrate, (b1, b2, b3, b4) Cu coating, (c1, c2, c3, c4) Cu-BNNSs coating

**Fig. 10** SEM images and EDS analysis of the wear surface of Cu-BNNSs composite coating



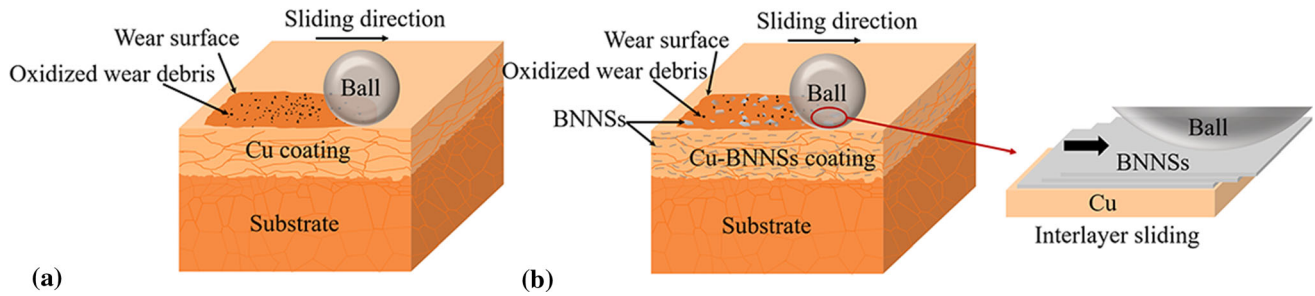


**Fig. 11** Schematic diagram of wear/friction behavior: (a) Cu coating (b) Cu-BNNSs composite coating

was beyond the sheet. This confirms that the small translucent sheet in Fig. 10(a) was BNNS.

The schematic diagrams of the wear and friction behavior of Cu and Cu-BNNSs composite coatings are depicted in Fig. 11. Clearly, the wear mechanism of both coatings is abrasive wear, with oxidized wear debris on the wear track (Fig. 11a and b). However, the presence of BNNSs makes a big difference: in the process of friction, BNNSs were gradually exposed and acted as a lubricant. The similar phenomenon is also reported in the literature (Ref 32, 40). The weak bonding between the BNNSs layers enables the interlayer sliding induced by the shearing between the countersurfaces and correspondingly reduces the friction coefficient (Ref 30). It is also worth noting that the flat BNNSs adhered to the worn surface can isolate the contact of ball and sample. This “protective film” improved the wear resistance effectively. Thus, there were few deep grooves on the composite coating.

## Conclusions

Copper and copper matrix composites reinforced by BNNSs were successfully deposited on the copper substrate by cold spray. According to the samples studied, the following points can be highlighted:

- BNNSs were widely distributed throughout the coating and no evident oxidation or phase transformation occurred during the fabrication process.
- Under the same spray conditions, the thickness and surface roughness of Cu-BNNSs composite coatings are smaller than those of Cu coating, because the existence of BNNSs hindered the adiabatic shear. Some particles cannot bond to the existing coating, but play the role of “shot peening”, making the coating surface flatter.

- The addition of BNNSs into the copper matrix could reduce the microhardness. There are some microcracks around the indents in Cu-BNNSs composite coating because of the de-bonding between the BNNSs and Cu particles.
- Tribological tests suggest that Cu-BNNSs composite coating has lower COF and wear rate than those of Cu substrate and Cu coating. BNNSs play the part of the lubricant and barrier, which improve the wear resistance of the coating.

**Acknowledgments** We acknowledge the financial support from Research Foundation for the National Natural Science Foundation of China [51575245, 51679112]; Senior Talent Foundation of Jiangsu University [18JDG030]; The Open Fund of Key Laboratory of Marine Materials and Related Technologies, CAS and Zhejiang Key Laboratory of Marine Materials and Protective Technologies [2020K06]. We acknowledge Yuelong Ma and Zhenqiang Liu for useful discussions.

## References

1. M.E. Lynch, W. Gu, T. El-Wardany, A. Hsu, D. Viens, A. Nardi and M. Klecka, Design and Topology/Shape Structural Optimisation for Additively Manufactured Cold Sprayed Components, *Virtual Phys. Prototyp.*, 2013, **8**(3), p 213-231.
2. O. Stier, Fundamental Cost Analysis of Cold Spray, *J. Therm. Spray Technol.*, 2013, **23**(1-2), p 131-139.
3. X.-T. Luo, Y.-K. Wei, Y. Wang and C.-J. Li, Microstructure and Mechanical Property of Ti and Ti6Al4V Prepared by an In-Situ Shot Peening Assisted Cold Spraying, *Mater. Des.*, 2015, **85**, p 527-533.
4. X.-T. Luo and C.-J. Li, Tailoring the Composite Interface at Lower Temperature by the Nanoscale Interfacial Active Layer Formed in Cold Sprayed cBN/NiCrAl Nanocomposite, *Mater. Des.*, 2018, **140**, p 387-399.
5. S. Grigoriev, A. Okunkova, A. Sova, P. Bertrand and I. Smurov, Cold Spraying: From Process Fundamentals Towards Advanced Applications, *Surf. Coat. Technol.*, 2015, **268**, p 77-84.
6. X.T. Luo, C.X. Li, F.L. Shang, G.J. Yang, Y.Y. Wang and C.J. Li, High Velocity Impact Induced Microstructure Evolution

- During Deposition of Cold Spray Coatings: A Review, *Surf. Coat. Technol.*, 2014, **254**, p 11-20.
7. N.H. Tariq, L. Gyansah, X. Qiu, H. Du, J.Q. Wang, B. Feng, D.S. Yan and T.Y. Xiong, Thermo-Mechanical Post-Treatment: A Strategic Approach to Improve Microstructure and Mechanical Properties of Cold Spray Additively Manufactured Composites, *Mater. Des.*, 2018, **156**, p 287-299.
  8. Z. Zhang, F. Liu, E.-H. Han, L. Xu and P.C. Uzoma, Effects of Al<sub>2</sub>O<sub>3</sub> on the Microstructures and Corrosion Behavior of Low-Pressure Cold Gas Sprayed Al 2024-Al<sub>2</sub>O<sub>3</sub> Composite Coatings on AA 2024-T3 Substrate, *Surf. Coat. Technol.*, 2019, **370**, p 53-68.
  9. E.J.T. Pialago and C.W. Park, Cold Spray Deposition Characteristics of Mechanically Alloyed Cu-CNT Composite Powders, *Appl. Surf. Sci.*, 2014, **308**, p 63-74.
  10. W. Chen, Y. Yu, J. Cheng, S. Wang, S. Zhu, W. Liu and J. Yang, Microstructure, Mechanical Properties and Dry Sliding Wear Behavior of Cu-Al<sub>2</sub>O<sub>3</sub>-Graphite Solid-Lubricating Coatings Deposited by Low-Pressure Cold Spraying, *J. Therm. Spray Technol.*, 2018, **27**(8), p 1652-1663.
  11. H. Che, X. Chu, P. Vo and S. Yue, Metallization of Various Polymers by Cold Spray, *J. Therm. Spray Technol.*, 2017, **27**(1-2), p 169-178.
  12. A. Vardelle, C. Moreau, J. Akedo, H. Ashrafizadeh, C.C. Berndt, J.O. Berghaus, M. Boulos, J. Brogan, A.C. Bourtsalas, A. Dolatabadi, M. Dorfman, T.J. Eden, P. Fauchais, G. Fisher, F. Gaertner, M. Gindrat, R. Henne, M. Hyland, E. Irissou, E.H. Jordan, K.A. Khor, A. Killinger, Y.-C. Lau, C.-J. Li, L. Li, J. Longtin, N. Markocsan, P.J. Masset, J. Matejicek, G. Mauer, A. McDonald, J. Mostaghimi, S. Sampath, G. Schiller, K. Shinoda, M.F. Smith, A.A. Syed, N.J. Themelis, F.-L. Toma, J.P. Trelles, R. Vassen and P. Vuoristo, The 2016 Thermal Spray Roadmap, *J. Therm. Spray Technol.*, 2016, **25**(8), p 1376-1440.
  13. W.-Y. Li, C.-J. Li and H. Liao, Effect of Annealing Treatment on the Microstructure and Properties of Cold-Sprayed Cu Coating, *J. Therm. Spray Technol.*, 2006, **15**(2), p 206-211.
  14. L. Zhang, S. Yang, X. Lv and X. Jie, Wear and Corrosion Resistance of Cold-Sprayed Cu-Based Composite Coatings on Magnesium Substrate, *J. Therm. Spray Technol.*, 2019, **28**(6), p 1212-1224.
  15. K. Rajkumar and S. Aravindan, Tribological Behavior of Microwave Processed Copper-Nanographite Composites, *Tribol. Int.*, 2013, **57**, p 282-296.
  16. C.J. Huang, H.J. Wu, Y.C. Xie, W.Y. Li, C. Verdy, M.P. Planche, H.L. Liao and G. Montavon, Advanced Brass-Based Composites via Cold-Spray Additive-Manufacturing and Its Potential in Component Repairing, *Surf. Coat. Technol.*, 2019, **371**, p 211-223.
  17. B.S. Ünlü and E. Atik, Evaluation of Effect of Alloy Elements in Copper Based CuSn10 and CuZn30 Bearings on Tribological and Mechanical Properties, *J. Alloy. Compd.*, 2010, **489**(1), p 262-268.
  18. Y. Wang, Z. Yin, G. Gao and X. Zhang, Analysis of the Performance of Worn Hydrodynamic Water-Lubricated Plain Journal Bearings Considering Cavitation and Elastic Deformation, *Mech. Ind.*, 2017, **18**(5), p 508.
  19. K.I. Triantou, D.I. Pantelis, V. Guipont and M. Jeandin, Microstructure and Tribological Behavior of Copper and Composite Copper+Alumina Cold Sprayed Coatings for Various Alumina Contents, *Wear*, 2015, **336-337**, p 96-107.
  20. Y. Zhang, J. Michael Shockley, P. Vo and R.R. Chromik, Tribological Behavior of a Cold-Sprayed Cu-MoS<sub>2</sub> Composite Coating During Dry Sliding Wear, *Tribol. Lett.*, 2016, **62**(1), p 1-12.
  21. Y. Zhang, S. Descartes, P. Vo and R.R. Chromik, Cold-Sprayed Cu-MoS<sub>2</sub> and Its Fretting Wear Behavior, *J. Therm. Spray Technol.*, 2015, **25**(3), p 473-482.
  22. J. Li, L. Gan, Y. Liu, S. Mateti, W. Lei, Y. Chen and J. Yang, Boron Nitride Nanosheets Reinforced Waterborne Polyurethane Coatings for Improving Corrosion Resistance and Antifriction Properties, *Eur. Polymer J.*, 2018, **104**, p 57-63.
  23. N. Kostoglou, K. Polychronopoulou and C. Rebholz, Thermal and Chemical Stability of Hexagonal Boron Nitride (h-BN) Nanoplatelets, *Vacuum*, 2015, **112**, p 42-45.
  24. W. Jin, L. Yuan, G. Liang and A. Gu, Multifunctional Cyclotriphosphazene/Hexagonal Boron Nitride Hybrids and Their Flame Retarding Bismaleimide Resins with High Thermal Conductivity and Thermal Stability, *ACS Appl. Mater. Interfaces.*, 2014, **6**(17), p 14931-14944.
  25. S.C. Yoo, J. Kim, W. Lee, J.Y. Hwang, H.J. Ryu and S.H. Hong, Enhanced Mechanical Properties of Boron Nitride Nanosheet/Copper Nanocomposites via a Molecular-Level Mixing Process, *Compos. Part B: Eng.*, 2020, **195**, p 108088.
  26. H. Chi, L. Jiang, G. Chen, P. Kang, X. Lin and G. Wu, Dry Sliding Friction and Wear Behavior of (TiB<sub>2</sub>+h-BN)/2024Al Composites, *Mater. Des.*, 2015, **87**, p 960-968.
  27. R.V.P. Kaviti, D. Jeyasimman, G. Parande, M. Gupta and R. Narayanasamy, Investigation on Dry Sliding Wear Behavior of Mg/BN Nanocomposites, *J. Magnesium Alloys*, 2018, **6**(3), p 263-276.
  28. J. Tharajak, T. Palathai and N. Sombatsompop, Morphological and Physical Properties and Friction/Wear Behavior of h-BN Filled PEEK Composite Coatings, *Surf. Coat. Technol.*, 2015, **273**, p 20-29.
  29. K.U. Yusupov, S. Corthay, A.V. Bondarev, A.M. Kovalskii, A.T. Matveev, D. Arkhipov, D.V. Golberg and D.V. Shtansky, Spark Plasma Sintered Al-Based Composites Reinforced with BN Nanosheets Exfoliated Under Ball Milling in Ethylene Glycol, *Mater. Sci. Eng., A*, 2019, **745**, p 74-81.
  30. D. Lee, B. Lee, K.H. Park, H.J. Ryu, S. Jeon and S.H. Hong, Scalable Exfoliation Process for Highly Soluble Boron Nitride Nanoplatelets by Hydroxide-Assisted Ball Milling, *Nano Lett.*, 2015, **15**(2), p 1238-1244.
  31. *Standard Guide for Preparation of Metallographic Specimens*, ASTM E3-11, ASTM International, 2017, p 1-13.
  32. Z.-S. Ma, H.-L. Ding, Z. Liu and Z.-L. Cheng, Preparation and Tribological Properties of Hydrothermally Exfoliated Ultrathin Hexagonal Boron Nitride Nanosheets (BNNs) in Mixed NaOH/KOH Solution, *J. Alloy. Compd.*, 2019, **784**, p 807-815.
  33. H. Yue, L. Yao, X. Gao, S. Zhang, E. Guo, H. Zhang, X. Lin and B. Wang, Effect of Ball-Milling and Graphene Contents on the Mechanical Properties and Fracture Mechanisms of Graphene Nanosheets Reinforced Copper Matrix Composites, *J. Alloy. Compd.*, 2017, **691**, p 755-762.
  34. W. Sun, A.W.-Y. Tan, A. Bhowmik, F. Xue, I. Marinescu and E. Liu, Evaluation of Cold Sprayed Graphene Nanoplates-Inconel 718 Composite Coatings, *Surf. Coatings Technol.*, 2019, **378**, p 125065.
  35. N. Nagabandi, C. Yegin, X. Feng, C. King, J.K. Oh, E.A. Scholar, S. Narumanchi and M. Akbulut, Chemically Linked Metal-Matrix Nanocomposites of Boron Nitride Nanosheets and Silver as Thermal Interface Materials, *Nanotechnology*, 2018, **29**(10), p 105706.
  36. W. Chen, Y. Yu, J. Ma, S. Zhu, W. Liu and J. Yang, Low-Pressure Cold Spraying of Copper-Graphite Solid Lubricating Coatings on Aluminum Alloy 7075-T651, *J. Therm. Spray Technol.*, 2019, **28**(7), p 1688-1698.
  37. O. Tazegul, O. Meydanoglu and E.S. Kayali, Surface Modification of Electrical Contacts by Cold Gas Dynamic Spraying Process, *Surf. Coat. Technol.*, 2013, **236**, p 159-165.

38. Y.J. Mai, F.X. Chen, W.Q. Lian, L.Y. Zhang, C.S. Liu and X.H. Jie, Preparation and Tribological Behavior of Copper Matrix Composites Reinforced with Nickel Nanoparticles Anchored Graphene Nanosheets, *J. Alloy. Compd.*, 2018, **756**, p 1-7.
39. S.B. Pitchuka, B. Boesl, C. Zhang, D. Lahiri, A. Nieto, G. Sundararajan and A. Agarwal, Dry Sliding Wear Behavior of Cold Sprayed Aluminum Amorphous/Nanocrystalline Alloy Coatings, *Surf. Coat. Technol.*, 2014, **238**, p 118-125.
40. X. Ci, W. Zhao and J. Luo, A Sustainable Interlayer Slip Leads to the Excellent Tribological Behaviour of Hexagonal Boron Nitride Microsheets, *Colloids Surf. A: Physicochem. Eng. Aspects*, 2020, **598**, p 124859.

**Publisher's Note** Springer Nature remains neutral with regard to jurisdictional claims in published maps and institutional affiliations.